SEPARATING MANIFOLDS IN SLOW-FAST SYSTEMS

Hinke M. Osinga and James P. England
Bristol Centre for Applied Nonlinear Mathematics
Department of Engineering Mathematics
University of Bristol, Bristol BS8 1TR, UK
H.M.Osinga@bristol.ac.uk, James.England@bristol.ac.uk

Abstract

There are many applications that lead to models involving different timescales. For example, this is particularly the case for models of neurons, which involve dynamics of ionic channels across the cell membrane. Due to the slow-fast nature of such models it is difficult to use numerical tools for the investigation of the global behaviour. This paper discusses the computation of global invariant manifolds for slow-fast systems. We explain how the different timescales cause the numerical difficulties and give suggestions on how to deal with these problems. We illustrate the techniques with the computation of separating manifolds in a Hodgkin-Huxley type model of a somatotroph cell; this is an endocrine cell in the anterior pituitary that secretes growth hormone. There are two co-existing attractors in this model and their basins of attraction are separated by global stable manifolds of equilibria or periodic orbits.

Key words

slow-fast systems, global invariant manifolds.

1 Introduction

There are many realistic phenomena that lead to models involving different timescales, for example mixed-mode oscillations in chemical reactions [Koper, 1995], self-pulsation in lasers [Dubbeldam and Krauskopf, 1999], or cell division cycles [Tyson, 1991]. Slow-fast systems can display dynamics not present in single-timescale ODEs, and have been used successfully to explain neuronal bursting mechanisms in biological systems [Golubitsky, Josić and Kaper, 2001].

The theory for slow-fast systems is still in its infancy and it is now generally recognised that progress will come by performing in-depth studies of specific examples, helped by advanced numerical techniques. In this paper we describe how to use the computation of two-dimensional global invariant stable or unstable manifolds in the investigation of slow-fast systems. While such computations are already challenging in single-timescale systems, we discuss the specific adaptations of the technique for systems with two or more timescales. As an illustrative example, we compute the global stable manifolds of saddle equilibria and periodic orbits in a simplified model of a somatotroph cell, a particular type of endocrine cell; see Section 2 for more details.

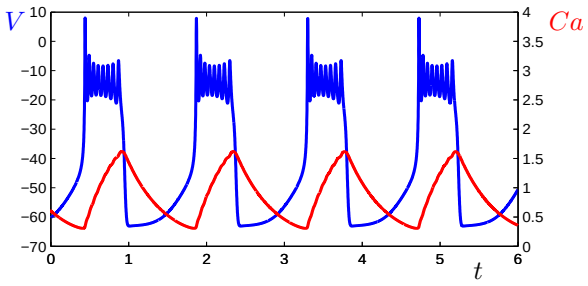

Figure 1. Numerical simulation of the voltage potential across the cell membrane (blue in mV) and the intracellular calcium concentration (red in μM) versus time (in s).

This paper is organised as follows. We begin by introducing the example used for the illustrations in Section 2. We then explain the algorithms for computing global invariant manifolds and discuss the difficulties for slow-fast systems in Section 3. We end with conclusions in Section 4.

2 Example of a slow-fast system

We illustrate our method with a model of bursting dynamics in a single somatotroph cell. This model is based on the Chay-Cook model [Chay and Cook, 1988] that was developed to simulate the electrical burst pattern of a pancreatic β-cell; it is discussed in detail in [Bertram, Butte, Kiemel and Sherman, 1995]. The cell fires membrane action potentials in bursts, consisting of regular trains of action potentials separated by silent periods during which the transmembrane potential is hyperpolarised. The termination of the burst, and the hyperpolarisation that follows, are believed to be the

result of an increase in intracellular Ca^{2+} ionic concentration. The dynamics of the transmembrane potential V and the Ca^{2+} concentration for the model used here is shown in Fig. 1

The voltage potential across the cell membrane is regulated by ionic currents. The membrane depolarises due to inward currents carried by Ca^{2+}. The termination of the spike train is due to the activation of a calcium-dependent outward potassium current, and this activation switches the membrane to hyperpolarisation. The model under consideration here describes the dynamics of the transmembrane potential V, involving the excitatory current I_{Ca}, the inhibitory current I_{K} and a passive leakage current I_{L}. The other variables are the intracellular free Ca^{2+} concentration Ca and two activation variables m and n that represent the fractions of open L-type calcium channels and delayed rectifier potassium channels, respectively. The basic format of the equations is then

$$\begin{cases} \dfrac{dV}{dt} = \dfrac{-1}{c_m}\,[I_{\mathrm{Ca}}(V,m) + I_{\mathrm{K}}(V,n) \\ \qquad\qquad +I_{\mathrm{KCa}}(V,Ca) + I_{\mathrm{L}}(V)], \\ \dfrac{dm}{dt} = \dfrac{m_\infty(V) - m}{\tau_m}, \\ \dfrac{dn}{dt} = \dfrac{n_\infty(V) - n}{\tau_n}, \\ \dfrac{dCa}{dt} = f\,[-\alpha\, I_{\mathrm{Ca}}(V,m) - k_c\, Ca]. \end{cases} \tag{1}$$

The functions $n_\infty(V)$ and $m_\infty(V)$ are of the form $(1+\exp[-(V-V_h)/S_h])^{-1}$, with constant half-maximal potential V_h and slope S_h. The term $\frac{1}{cm} = 10^3\,\pi^{-1}$ indicates that the variation in the V-coordinate happens at a timescale that is about 300 times faster than the timescales for m and n. In contrast, the Ca-coordinate varies on a timescale that is at least 10 times slower than those for m and n. The full details of the model will be published elsewhere.

The dynamics of the model is characterised by the very fast behaviour of V and the slow variation of Ca when compared with m and n. In order to explain the burst pattern, it is standard to consider the *fast subsystem* obtained by considering the limit $\frac{d}{dt}Ca = 0$. The bifurcation diagram of the three-dimensional fast subsystem predicts the burst pattern as is shown in Fig. 2 where the burst pattern (black) is projected onto the bifurcation diagram in the (Ca, V)-plane; see [Jones, 1995] for more details on how to analyse slow-fast systems. The Ca^{2+} concentration decreases for small V (hyperpolarisation phase) and increases for large V (depolarisation phase). These two phases are stable equilibria in the fast subsystem that coexist for a small range of Ca-values marked by a saddle-node (label SN, $Ca \approx 0.355$) and a (subcritical) Hopf bifurcation (label H, $Ca \approx 1.919$); the spikes of the bursting oscillation are generated by the unstable periodic solutions of the fast subsystem. These periodic solution exist before the Hopf bifurcation and are created in a homoclinic bifurcation at $Ca \approx 0.701$ (label Hom) of the saddle equilibrium in between the two stable equlibria; see Fig. 2. We refer to [Bertram, Butte, Kiemel and Sherman, 1995] for more details on this type of bursting.

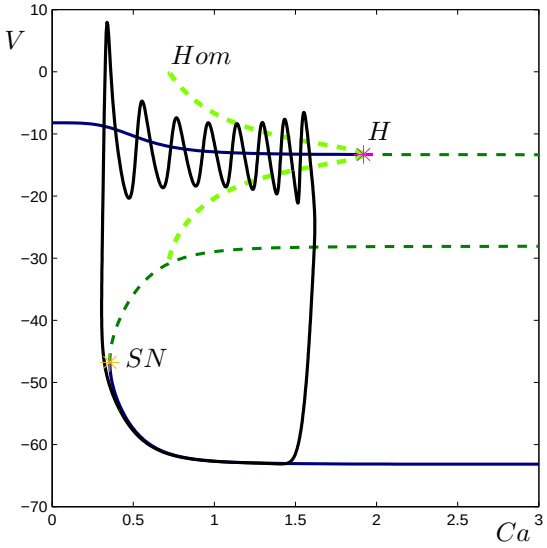

Figure 2. Bifurcation diagram of the fast subsystem, where Ca is a parameter. Stable equilibria are shown in blue; both maximal and minimal values of the periodic orbits are drawn.

The focus of study for this model is the so-called phase resetting. We consider here specifically the case of shortened hyperpolarisation, which means that the system is perturbed during the hyperpolarisation phase so that the state of the system is brought up prematurely to the depolarisation phase after which it continues its cyclic behaviour. This results in a left-phase shift of the bursting pattern. The perturbation is obtained by applying an additional current $I_{\mathrm{app}}(t)$ to the equation of V in (1) in the form of a (short) step function. This reflects the experimental manipulation that one could use to test resetting in the different types of endocrine cells in the brain.

A first requirement for successful phase resetting would be that the perturbation is such that it pushes the hyperpolarised state into the basin of attraction of the depolarised state for the same Ca-value. In between the saddle-node and the homoclinic bifurcation, this basin is bounded by the two-dimensional stable manifold of the saddle equilibrium that is created in the saddle-node bifurcation. After the homoclinic bifurcation, the separatrix is the stable manifold of the saddle periodic orbit. Since the saddle periodic orbit shrinks to a point at the Hopf bifurcation, the basin is becoming smaller and smaller as Ca increases.

In this paper we discuss the computation of such separating manifolds using two complementary algorithms. This is illustrated with the stable manifolds for several values of Ca.

3 Computing invariant manifolds

We consider two approaches for computing the invariant manifolds of the saddle equilibrium or periodic orbits of the three-dimensional fast subsystem of (1). Namely, we discuss the computation of the full two-dimensonal manifolds in the three-dimensional vector field in Sec. 3.1. We also describe in Sec. 3.2 the computation of the one-dimensional intersections of these manifolds with a suitably chosen plane. These one-dimensional intersections can be interpreted as the invariant manifolds of fixed points of the Poincaré map or first return map defined on this plane.

3.1 Two-dimensional manifolds of a vector field

Even in single-timescale ODEs, the development of numerical methods for the computation of invariant manifolds is recent; see [Krauskopf, Osinga, Doedel, Henderson, Guckenheimer, Vladimirsky, Dellnitz, and Junge, 2005] for an overview of available algorithms. The computations in this paper were done with the algorithm in [Krauskopf and Osinga, 1999, 2003] that uses the idea of growing the manifold as a collection of geodesic level sets. That is, the method computes a two-dimensional manifold of an equilibrium or periodic orbit as a collection of topological circles consisting of points that all lie at the same geodesic distance (shortest path along the manifold) to the equilibrium or periodic orbit.

To compute, say, the two-dimensional stable manifold of a saddle equilibrium, one starts with a circle of uniformly distributed mesh points in the stable eigenspace centered at the saddle point and with small radius. The algorithm now adds new topological circles to the data set that are approximations of geodesic level sets on the stable manifold as follows. For each mesh point r on the last computed level set we associate a new mesh point b_r on the level set at distance Δ away. In order to ensure a nice distribution on this new geodesic level set, b_r is chosen such that it lies itself at (geodesic) distance Δ from r. This means that b_r lies in a (hyper)plane $\mathcal{F}_r$ through r, perpedicular to the last computed level set. We find the point b_r by solving a boundary value problem. Namely, locally near r there is a unique one-dimensional curve on $\mathcal{F}_r$ of points that under forward integration eventually reach the last computed level set. That is, these points lie on the stable manifold. The boundary value problem is now formulated as those solutions $\mathbf{x}(t)$ to the vector field that satisfy the boundary conditions

$$\begin{aligned} &\mathbf{x}(0) \in \mathcal{F}_r, \\ &\mathbf{x}(\tau) \in \text{last computed level set}, \end{aligned}$$

where τ is the total integration time needed to reach the last computed level set. Note that the one-dimensional curve is, in fact, parametrised by the total integration time τ. The mesh point r solves the boundary value problem with $\tau = 0$ and τ increases as we follow the curve away from r. The boundary value problem is solved in a continuation setting, starting from the known solution $\mathbf{x}(t) = r$, $0 \leq t \leq \tau$, with $\tau = 0$. We follow the solution until τ is such that $\| \mathbf{x}(\tau) - r \| = \Delta$.

The above computation is done for all mesh points, and possibly other points that are interpolated in between the mesh points on the last computed level set if the new mesh points lie too far apart. This way the manifold can be grown as long as the geodesic level sets are well-defined topological circles, that is, they have no self-intersections; see [Krauskopf and Osinga, 1999, 2003] for more details.

The boundary value solver for this algorithm is at present only implemented using a relatively simple shooting method. In the context of slow-fast systems the integration is done with the Shampine stiff solver from [Press, Teukolsky, Vetterling and Flannery, 1992]. As mentioned in Sec. 2, one of the coordinates in the fast subsystem of our example is approximately 300 times faster than the other two. The stiff solver is able to integrate initial conditions for this system provided the total integration time is reasonably long. Since the algorithm uses trajectory segments of similar length to determine new mesh points, the total integration time decreases dramatically as the geodesic distance to the equilibrium or periodic orbit gets larger. Hence, this could be a serious problem outside a neighbourhood of the saddle-type object.

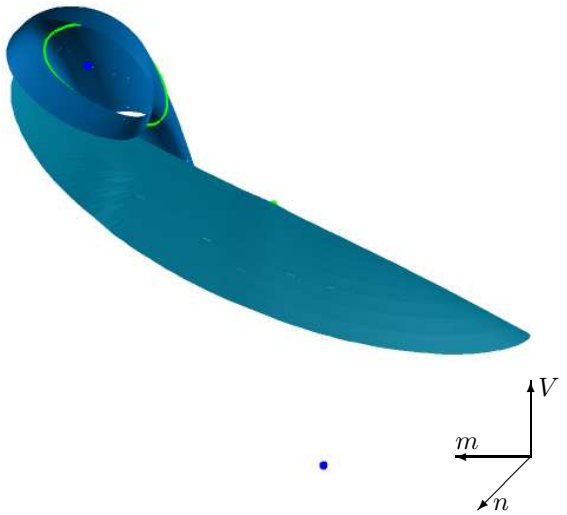

Figure 3. The stable manifolds of the saddle equilibrium and periodic orbit for $Ca = 1.0$.

Figure 3 shows the stable manifolds of the saddle equilibrium and the periodic orbit for $Ca = 1.0$. The viewpoint is chosen such that the V-axis is the vertical axis in this figure. The figure clearly shows that a perturbation from the hyperpolarised state, near the stable equilibrium at the bottom (blue point), just in the V-coordinate will not push the state into the basin of attraction of the depolarised state. Namely, this basin is inside the tube formed by the stable manifold of the

saddle periodic orbit. This means that it is impossible to achieve phase resetting by an instantaneously applied current.

During the computations we used a weighted norm to determine the geodesic level sets, because m and n are fractions between 0 and 1, and V is of order 10^2. More precisely, m was multiplied by 100 and n by 500. In this weighted norm, the stable manifold of the saddle was computed up to geodesic distance 53. This is the moment where the algorithm breaks down, due to problems with solving the boundary value problem. It is important to use an accurate boundary value solver and the difficulties of the computation seem to be entirely due to the shooting method that we use. We are currently working on an implementation using the boundary value solver of AUTO [Doedel, Paffenroth, Champneys, Fairgrieve, Kuznetsov, Oldeman, Sandstede and Wang, 2000].

There is an additional difficulty that seems typical for slow-fast systems. Namely, the two stable eigenvalues of the saddle equilibrium are very negative leading to extreme stretching when integrating backward in time. In the example with $Ca = 1.0$, the two stable eigenvalues are approximately -41.29 and -528.87. The order of 10 in the ratio of these eigenvalues is another factor that makes the computation of the stable manifold a challenge. On the other hand, the unstable eigenvalue is approximately 98.58, which means that the error transverse to the manifold is rapidly decreasing as the manifold is grown, at least close to the equilibrium.

The stable manifold of the saddle periodic orbit needs the linear eigenbundle associated with the stable Floquet multiplier as start data. We use AUTO to find this eigenbundle by solving for the first variational equation together with the dynamical system. The boundary conditions for the periodic orbit are as usual, while those for the linear eigenbundle $\mathbf{u}(\cdot)$ are of the form

$$\mathbf{u}(1) = \lambda\, \mathbf{u}(0),$$

where the period of the orbit is rescaled to 1. These boundary conditions are solved for arbitrary λ if the vector bundle is trivial. However, AUTO detects a branching bifurcation at the appropriate Floquet multiplier and the nontrivial bundle is found by switching branches here. For the example with $Ca = 1.0$ the unstable Floquet multiplier is approximately 1.48, but it is very difficult to determine the stable Floquet multiplier accurately. It appears to be of the order of 10^{-24}. However, it is our experience that the linear eigendirections obtained from solving the boundary value problem in AUTO are accurate even when the Floquet multiplier is not.

The difficulties in computing the stable manifold of the saddle periodic orbit are otherwise of a similar nature to those for the saddle fixed point. For $Ca = 1.0$ the algorithm appears to breaks down due to the problem of solving the boundary value problem with shooting. This happens at geodesic distance 70.8 for one side of the manifold and at 38.58 for the other. In fact, for other Ca-values we have sometimes only been able to calculate part of one side of the stable manifold. We expect that these difficulties will be overcome substantially when using the boundary value solver of AUTO.

3.2 One-dimensional manifolds in a plane

The second algorithm, which we developed only recently, computes intersections of the separating manifolds with a suitably chosen Poincaré section. The two-dimensional global stable manifold of a saddle periodic orbit is computed as the one-dimensional global stable manifold of the saddle fixed point of a Poincaré map, obtained by integrating points on a specified plane or Poincaré section transverse to the periodic orbit until the trajectory returns to this section. This technique is often used for the local analysis in a neighbourhood of the periodic orbit. This is due to the fact that the Poincaré map is often only locally a well-defined diffeomorphism. The only exception is when the vector field is equivalent to a periodically forced system [Yang, 2000]. Otherwise, the vector field will become tangent to the Poincaré section at points outside a neighbourhood of the periodic orbit, and the Poincaré map will be discontinuous at such points.

The method is closely related to the algorithms described in [Krauskopf and Osinga, 1998; England, Krauskopf and Osinga, 2004, 2005] that are for the computation of one-dimensional manifolds of discrete dynamical systems. That is, the manifolds are calculated in the same way using the associated Poincaré map for defining the discrete system. However, the Poincaré map is not determined by integrating particular point in the Poincaré section until it returns. Instead, we formulate the Poincaré map as a two-point boundary value problem and work with trajectory segments in the full state space that have both boundary points in the section.

The starting point is the saddle periodic orbit, formulated as the solution of a boundary value problem with boundary points in the Poincaré section. For this particular solution, the boundary points are equal, but a family of non-periodic solutions exists that do still have both boundary points in the section. We trace a one-dimensional branch of such solutions by letting the first boundary point follow initially the linear eigendirection in the Poincaré secion that is associated with the stable Floquet multiplier. The end point then traces a part of the stable manifold and as it curves away from the linear eigendirection, we switch and restrict the first boundary point of the solution to this segment. In this manner a large part of the global stable manifold can be found. This algorithm was implemented using the two-point boundary value solver of AUTO. We refer to [England, Krauskopf and Osinga, 2005] for more details.

The main advantage of this method is that the usual problems with integrating initial conditions in slow-fast systems, that were already pointed out in Sec. 3.1, are

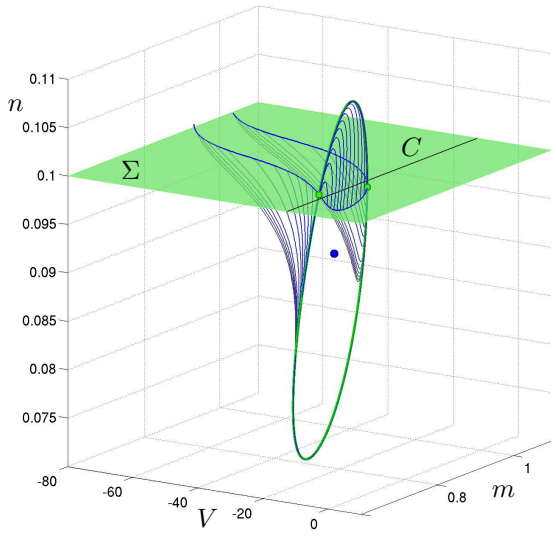

Figure 4. The one-dimensional stable manifold of the saddle periodic orbit for $Ca = 1.25$ in the Poincaré section $\Sigma = \{n = 0.1\}$. Some of the trajectory segments used for the computation are shown. Notice the change in transverse direction of the flow on either side of the curve $C = \{n = 0.1, V \approx -12.58\}$ along which the associated Poincaré map is discontinuous.

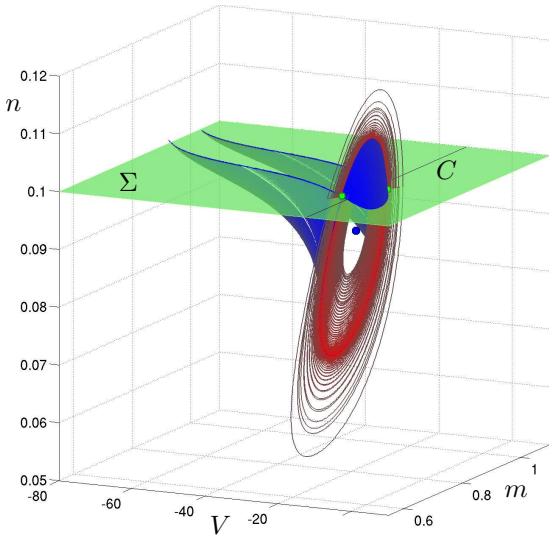

Figure 5. The trajectory segments used for computing the one-dimensional stable (blue) and unstable (red) manifolds of the saddle periodic orbit for $Ca = 1.25$ in the Poincaré section $\Sigma = \{n = 0.1\}$. One side of the two-dimensional unstable manifold accumulates on the stable equilibrium corresponding to the depolarisation state.

dealt with by the boundary value solver. The collocation methods used in AUTO are far more accurate and make it possible to find the typically long curves traced out by the end points of solutions for which the first boundary point varies ever so slightly. Furthermore, by continuing the boundary value problem, this method is able to cross over discontinuity curves.

As an example we computed the stable manifold of the saddle periodic orbit of the fast subsystem of (1) with $Ca = 1.25$ in the Poincaré section $\Sigma = \{n = 0.1\}$. The saddle periodic orbit intersects Σ at two points that can be considered as fixed points of the Poincaré map defined as the second return to the section. The vector flow is tangent to Σ when

$$\frac{dn}{dt} = 0 \Leftrightarrow \frac{n_\infty(V) - n}{\tau_n} = 0 \Leftrightarrow$$
$$n = n_\infty(V) = \frac{1}{1 + \exp[-(V - V_n)/S_n]} \Leftrightarrow$$
$$V \approx -12.58,$$

where $V_n = 5.0$ and $S_n = 8.0$ are given constants. This is the curve labelled C in Fig. 4.

As we calculate the one-dimensional stable manifold of one of the two fixed points, the algorithm will solve the two-point boundary value problem first as a family of solution segments that begin and end in Σ with one extra intersection with Σ in between (the second-return Poincaré map). As this solution branch passes through C, the solution segments pick up a third intersection, while the begin point is traced back towards the fixed point. The computation stops when the other fixed point is reached. As can be seen in Fig. 4 this results in a branch of the stable manifold in Σ that connects the two intersection points of the saddle periodic orbit. The other two branches eventually connect as well, but this is not shown in the figure.

Figure 5 shows the intersections of both the stable and unstable manifolds of the saddle periodic orbit for $Ca = 1.25$ with $\Sigma = \{n = 0.1\}$. All trajectory segments used in the computation are shown here, giving a fairly good impression of the two-dimensional manifolds. One side of the two-dimensional unstable manifold accumulates on the stable equilibrium that represents the depolarised state, as is expected from the subcritical Hopf bifurcation at larger Ca-value. The other side of this manifold forms a heteroclinic connection with the two-dimensional stable manifold of the saddle equilibrium. As a result, the one-dimensional intersection with Σ is only a short curve segment that ends at a point where the stable manifold of the saddle equilibrium intersects Σ. The algorithm cannot compute past such a heteroclinic orbit.

Figure 6 shows the intersections of both the stable and unstable manifolds of the saddle periodic orbit for $Ca = 0.84$ with $\Sigma = \{n = 0.05\}$. The vector field is now tangent to Σ at $V \approx -18.56$. One side of the two-dimensional unstable manifold of the saddle periodic orbit again accumulates on one of the two stable equilibria. However, since Σ is so far below this equilibrium, the orbits used in the computation do not come as close to this equilibrium as for $Ca = 1.25$ with $n = 0.1$; see also Fig. 5. On the other hand, Σ lies much closer to the saddle equilibrium, which is reflected in the sharp turn made by the trajectory seg-

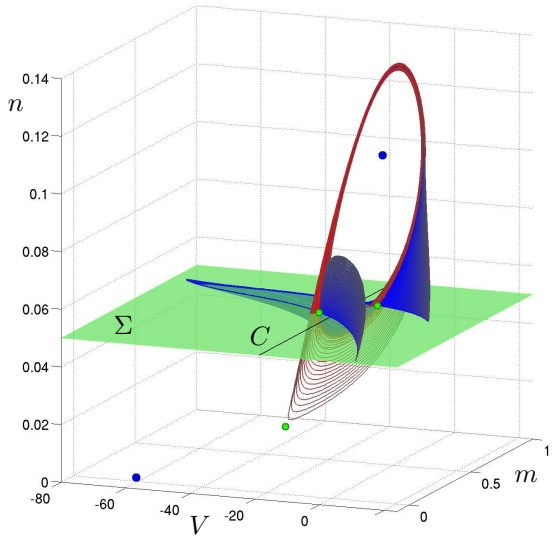

Figure 6. The trajectory segments used for computing the one-dimensional stable (blue) and unstable (red) manifolds of the saddle periodic orbit for $Ca = 0.84$ in the Poincaré section $\Sigma = \{n = 0.05\}$. The saddle equilibrium and the two stable equilibria corresponding to the hyperpolarised and depolarised states are shown as well.

ments for the computation of the other side of the two-dimensional unstable manifold of the saddle periodic orbit. These orbits lie much closer to the heteroclinic connection that exists between this manifold and the two-dimensional stable manifold of the saddle equilibrium. Furthermore, the value for Ca is much closer to the homoclinic bifurcation at $Ca \approx 0.701$ so that the two-dimensional stable manifold of the saddle equilibrium is already quite close to the periodic orbit. Hence, there is only a very short segment of the unstable manifold in Σ up to the heteroclinic connection.

4 Discussion

We presented two complementary methods for calculating two-dimensional global stable (or unstable) manifolds of saddle equilibria or periodic orbits in slow-fast systems. The method in Sec. 3.1 computes the manifolds as two-dimensional manifolds in the full state space. The method in Sec. 3.2 considers only the one-dimensional intersections of the manifolds with a suitably chosen Poincaré section.

The computations remain challenging due to the difference in timescales, but some of the numerical difficulties can be overcome by avoiding the use of shooting methods and work with two-point boundary value solvers instead. The algorithm used in Sec. 3.1 breaks down due to problems with the shooting method. We are currently working on an implementation that uses the two-point boundary value solver of AUTO [Doedel, Paffenroth, Champneys, Fairgrieve, Kuznetsov, Oldeman, Sandstede and Wang, 2000] and expect this to lead to a great improvement in performance. The algorithm used in Sec. 3.2 already uses AUTO for solving the two-point boundary value problem. Standard shooting methods do not work at all here, because most initial conditions never return to the chosen Poincaré section. This method seems even more sensitive to the numerics, because the stable Floquet multiplier of the saddle periodic orbit is extremely close to 0, a property that seems typical for slow-fast systems.

Acknowledgments

This work is part of an ongoing research collaboration with Arthur Sherman and Julie Stern at the National Institutes of Health, Bethesda, USA. We would like to thank both Arthur and Julie for many helpful discussions and their detailed explanations about the model. The research of J.E. was supported by grant GR/R94572/01 from the Engineering and Physical Sciences Research Council (EPSRC).

References

Bertram, R., Butte, M. J., Kiemel, T. and Sherman, A. [1995] Topological and phenomenological classification of bursting oscillations. *Bull. Math. Biol.* **57**(3), pp. 413–439.

Chay, T. R. and Cook, D. L. [1988] Endogenous bursting patterns in excitable cells. *Math. Biosci.* **90**, pp. 139–153.

Doedel, E. J., Paffenroth, R. C., Champneys, A. R., Fairgrieve, T. R., Kuznetsov, Yu. A., Oldeman, B. E., Sandstede, B. and Wang, X. J. [2000] AUTO2000: Continuation and bifurcation software for ordinary differential equations. available via `http://cmvl.cs.concordia.ca/`.

Dubbeldam, J. L. A. and Krauskopf, B. [1999] Self-pulsations in lasers with saturable absorber: dynamics and bifurcations. *Optics Communications* **159**(4-6). pp. 325–338.

England, J. P., Krauskopf, B. and Osinga, H. M. [2004] Computing one-dimensional stable manifolds of planar maps without the inverse. *SIAM J. Appl. Dyn. Sys.* **3**(2), pp. 161–190.

England, J. P., Krauskopf, B. and Osinga, H. M. [2005] Computing one-dimensional global manifolds of Poincaré maps by continuation. Applied Nonlinear Mathematics Preprint **2005.03**.

Golubitsky, M., Josić, K. and Kaper, T. J. [2001] An unfolding theory approach to bursting in fast-slow systems. In Broer, H. W., Krauskopf, B. and Vegter, G. (Eds.) *Global Analysis of Dynamical Systems*. Festschrift dedicated to Floris Takens for his 60^{th} birthday, pp. 277–308, IoP Publishing, Bristol.

Jones, C. K. R. T. [1995] *Geometric Singular Perturbation Theory*. C.I.M.E. Lectures, Montecatini Terme, June 1994, Lecture Notes in Mathematics **1609**, Springer-Verlag, Heidelberg.

Koper, M. T. M. [1995] Bifurcations of mixed-mode oscillations in a three-variable autonomous Van der

Pol-Duffing model with a cross-shaped phase diagram. *Physica* **D80**, pp. 72–94.

Krauskopf, B. and Osinga, H. M. [1998] Growing 1D and quasi 2D unstable manifolds of maps. *J. Comp. Phys.* **146**(1), pp 404–419.

Krauskopf, B. and Osinga, H. M. [1999] Two-dimensional global manifolds of vector fields. *CHAOS* **9**(3), pp 768–774.

Krauskopf, B. and Osinga, H. M. [2003] Computing geodesic level sets on global (un)stable manifolds of vector fields. *SIAM J. Appl. Dyn. Sys.* **2**(4), pp. 546–569.

Krauskopf, B. and Osinga, H. M., Doedel, E. J., Henderson, M. E., Guckenheimer, J., Vladimirsky, A., Dellnitz, M. and Junge, O. [2005] A survey of methods for computing (un)stable manifolds of vector fields. to appear in *Int. J. Bifurcation and Chaos* **15**(3).

Press, W. H., Teukolsky, S. A., Vetterling, W. T. and Flannery, B. P. [1992] *Numerical Recipes in C*. Cambridge University Press, 2nd edition.

Sherman, A. [1997] Calcium and membrane potential oscillations in pancreatic beta-cells. In Othmer, H. G., Adler, F. R., Lewis, M. A. and Dallon, J. C. (Eds.) *Case Studies in Mathematical Modeling - Ecology, Physiology, and Cell Biology*, pp. 199–217, Prentice-Hall, New Jersey.

Tyson, J. J. [1991] Modeling the cell division cycl:cdc2 and cyclin interactions. *Proc. Nat. Acad. Sci. U.S.A.* **88**, pp. 7328–7332.

Yang, X. S. [2000] A remark on global Poincaré section and suspension manifold. *Chaos Solitons and Fractals* **11**, pp. 2157–2159.